Journal of Quantitative Spectroscopy & Radiative Transfer 113 (2012) 951–960

Contents lists available at SciVerse ScienceDirect

Journal of Quantitative Spectroscopy & Radiative Transfer

journal homepage: www.elsevier.com/locate/jqsrt

Comparison of trajectory models in calculations of N_2-broadened half-widths and N_2-induced line shifts for the rotational band of $H_2{}^{16}O$ and comparison with measurements

J. Lamouroux [a,b], R.R. Gamache [a,b,*], A.L. Laraia [a,b], Q. Ma [c], R.H. Tipping [d]

[a] University of Massachusetts, School of Marine Sciences, MA 01854-5045, USA
[b] University of Massachusetts Lowell, Department of Environmental, Earth, and Atmospheric Sciences, One University Avenue, Lowell, MA 01854-5045, USA
[c] NASA/Goddard Institute for Space Studies, Department of Applied Physics and Applied Mathematics, Columbia University, 2880 Broadway, NY 10025, USA
[d] Department of Physics and Astronomy, University of Alabama, Tuscaloosa, AL 35487, USA

ARTICLE INFO

Available online 25 November 2011

Keywords:
Water vapor
H_2O
Complex Robert–Bonamy formalism
Trajectory models
Half-widths
Line shifts
Hamilton's equations of motion

ABSTRACT

In this work, Complex Robert–Bonamy calculations of half-widths and line shifts were done for N_2-broadening of water for 1639 transitions in the rotational band using two models for the trajectories. The first is a model correct to second order in time, the Robert–Bonamy parabolic approximation. The second is the solution of Hamilton's equations. Both models use the isotropic part of the atom–atom potential to determine the trajectories. The present calculations used an intermolecular potential expanded to 20th *order* to assure the convergence of the half-widths and line shifts. The aim of the study is to assess if the difference in the half-widths and line shifts determined from the two trajectory models is greater than the accuracy requirements of the spectroscopic and remote sensing communities. The results of the calculations are compared with measurements of the half-widths and line shifts. It is shown that the effects of the trajectory model greatly exceed the needs of current remote sensing measurements and that line shape parameters calculated using trajectories determined by solving Hamilton's equations agree better with measurement.

1. Introduction

Since the pioneer works of Anderson [1,2] (ATC) and Tsao and Curnutte [3], several semiclassical theoretical models were developed to predict the pressure-broadening parameters [4–6] (and references therein). Within these theories, the relative motions of the perturber and the radiator (trajectories) are described classically and often parameterized by the molecular interaction potential used to describe the molecular collisions through various classical dynamics models. In the ATC theory, the bending of the trajectories due to the stronger interaction at close distances was not taken into account and simple straight paths with constant relative velocity were used. Moreover to insure physical behavior of the theory requires an unphysical cutoff be applied at small impact parameters. In the semiclassical Quantum Fourier Transform (QFT) theory [7,8], the cutoff parameter was adjusted so that the theoretical calculations agree with measured values for high and intermediate *J* lines [8]. This model leads to good predictions for systems where electrostatic interactions are dominant ("strong-collision" systems), however inaccurate results are obtained when close collisions are important, i.e. weak interacting systems. Here the notion of strong and weak collision systems adopts the definition of Oka [9].

Several developments have focused on building cutoff-free theories and, in general, improving the molecular

* Corresponding author at: University of Massachusetts, School of Marine Sciences, MA 01854-5045, USA. Tel.: +1 978 934 3904; fax: +1 978 934 3069.
E-mail address: Robert_Gamache@uml.edu (R.R. Gamache).

0022-4073/$ - see front matter © 2011 Elsevier Ltd. All rights reserved.
doi:10.1016/j.jqsrt.2011.11.010

dynamics models [10–22]. Herman and Tipping [10–12] considered approximate curved trajectories determined by an isotropic intermolecular Lennard–Jones potential. An isotropic potential was also used within the approach developed by Neilsen and Gordon [13] but the computation time required made it unusable for practical applications. A similar dynamical model was used by Smith et al. [14], however the peaking approximation made this theory inaccurate at very low quantum numbers. In the formalism developed by Robert and Bonamy (RB) [16], the cutoff procedure was eliminated through the application of the linked-cluster techniques and the cumulant expansion [23]. The RB model introduced a short-range atom–atom potential and an analytical trajectory model (correct to second order in time) defined by the isotropic part of the atom–atom potential. Since its development for linear active molecule perturbed by a linear molecule or an atom, the RB formalism has been extended to asymmetric and symmetric top [24–26], and spherical top molecules [27–30]. The extension using a complex implementation (CRB) [31] allows the calculation of the pressure-broadening parameters through a single calculation that takes into account simultaneously the real and imaginary components of the scattering matrix. The RB and CRB calculations of broadening-pressure parameters were performed for numerous molecular systems, one can refer to Refs. [5,6] and references therein for a detailed bibliography. These studies using curved trajectories based on the isotropic part of the intermolecular potential show improvement of the calculations relative to the straight path model.

Due to the improvement in computational resources, the influence of real trajectories can be studied using the so-called "exact" trajectory models based on the classical dynamic equations of motion [32] (Hamilton's equations). Bykov et al. [33] (and references therein) proposed an exact solution of Hamilton's equations based on a universal function of two arguments, which is independent of the parameters of potential and initial conditions of the collisions, allowing the general solution to then be applied to collision systems where long-range interactions are dominant. Joubert et al. [34] and Buldyreva et al. [35–38] made calculations using this formalism for several molecular systems. "Exact" trajectories can also be obtained by the numerical integration of Hamilton's equations of motion. RB calculations for self-broadening of CO and N_2 were done using several "exact" trajectory models by Afzelius et al. [38]. Within the CRB framework, Neshyba and Gamache [39] made calculations for N_2-broadening of $\sim$10 water vapor transitions using both the parabolic model of Robert and Bonamy and the "exact" trajectory model by solving Hamilton's equations. They found less than a percent difference between the half-widths from the two methods of calculation. Antony et al. [40] have calculated the half-widths of self-broadening of H_2O using the numerical integration of Hamilton's equations, however they found no significant differences between the parabolic and the "exact" model for this strong-collision system. Despite the fact that these procedures are more time consuming than approximate trajectories, as numerical integration is required at each point of the trajectory, they do yield more realistic trajectories. It has also been found that the RB parabolic model is inappropriate for some collision systems, e.g. CO_2–N_2 or CO_2–O_2 [41,42].

Water vapor plays a crucial role in the terrestrial atmosphere and in interstellar space [43]. In the Earth's atmosphere, H_2O is the strongest absorber of infrared radiation [44]. From remote sensing measurements one can determine the temperature, pressure, and concentration profiles for all the major gases present in the atmosphere if the spectroscopic parameters (positions, intensities, half-widths, line shifts, and temperature dependence) are known. These parameters are available from databases such as HITRAN [45] or GEISA [46]. Among the parameters used for the inversion of the remote sensing measurement, the half-widths and line shifts are those with the largest uncertainty. Several studies of the 22 and 183 GHz lines of water vapor [47–49] have shown that small changes in the pressure-broadened parameters can yield significant improvements in retrieved profiles. Due to its importance for the Earth's atmosphere, numerous measurements (Ref. [50] and references therein) and calculations [5,6,51–55] of the pressure-broadened parameters have been done for self, N_2, O_2, and air broadening of water vapor. The improvement of both experimental techniques and semiclassical theories has shown that small effects previously considered as insignificant may be important to meet the requirements of the spectroscopic and remote sensing community [56–58]. The inclusion of the imaginary components in the calculations of the half-widths is an example. The mean-relative thermal velocity approximation has been used in almost all the calculations, despite the fact that studies have shown [59,60] the importance of explicitly averaging over the Maxwell–Boltzmann distribution. Similarly, the question of the influence of vibration on the half-widths of water vapor was considered in previous studies [61–65], a survey paper [66], and several workshops [56–58] that estimated that the effect of the vibrational states of the transition was smaller than experimental uncertainties. A study by Gamache and Hartmann [67] demonstrated, for the first time, a clear vibrational dependence of the half-widths for certain classes of transition in both the measured and calculated data. The effects mentioned above must now be considered if the calculations are to meet the needs of the spectroscopic and remote sensing communities.

Similar questions arise regarding the influence of the trajectory models on the half-widths and line shifts. While some studies have shown no difference between the two models [39,40], these studies considered only a small number of broad lines (large half-width). In 2009, in a study of some transitions in the rotational band of water broadened by nitrogen, Tipping and Ma [68] found the difference can reach about 10%.

In a recent work [69], the question of trajectory models was addressed for the half-widths. The present study extends this work using a higher *order* expansion of the intermolecular potential as recommended by Ma et al. [22], considers the line shifts, explains some of the observed features in more detail, and compares the calculations with measurement. CRB calculations using trajectories obtained from solving Hamilton's equations and from the parabolic approximation were made and the

results compared with each other and with measurement. The two trajectory models are compared with the needs of the remote sensing community in mind.

2. Theory

2.1. The complex Robert–Bonamy formalism

The Complex Robert–Bonamy formalism (CRB) used for the calculations is described in details in Refs. [31,70–72], only the main features are given here. Within this formalism, the half-width, γ, and line shift, δ, of a ro-vibrational transition $f \leftarrow i$ are obtained from a single calculation by the real and minus the imaginary part of

$$(\gamma - i\delta)_{f\leftarrow i} = \frac{n_2}{2\pi c} \langle v[1 - e^{-{}^{R}S_2(f,i,J_2,v,b)} e^{-i({}^{I}S_1(f,i,J_2,v,b) + {}^{I}S_2(f,i,J_2,v,b))}] \rangle_{v,b,J_2} \quad (1)$$

where n_2 is the number density of perturbers, c the speed of light, and $\langle\ \rangle_{v,b,J_2}$ represents an average over all trajectories (impact parameter b and initial relative velocity v) and initial rotational state J_2 of the collision partner. S_1 and $S_2 = {}^{R}S_2 + i{}^{I}S_2$ are, respectively, the first and the second order terms in the successive expansion of the Liouville scattering matrix, S. They depend on the ro-vibrational states involved and associated collision induced jumps from these levels, and on the intermolecular potential and characteristics of the collision dynamics. Note that since there is no change in the vibrational state, the S_1 term vanishes. Within the semiclassical CRB formalism, the S_2 terms can be written as the product of reduced matrix elements (quantum mechanical component) for the perturber and the radiator and the resonances functions (classical component). The exact forms of these terms can be found in Refs. [70–72].

The wavefunctions used to evaluate the reduced matrix elements are obtained by diagonalizing the Watson Hamiltonian [73] in a symmetric top basis. The wavefunctions for the ground vibrational state are determined using the constants of Matsushima et al. [74]. The molecular rotation constants for N_2 are from Huber and Herzberg [75].

The intermolecular potential used in the calculations is a sum of an electrostatic component (dipole and quadrupole moments of H_2O with the quadrupole moment of N_2) and an atom–atom component. Many of the molecular parameters for the H_2O–N_2 system are well known and the present calculations use the best available values from the literature [76–79]. The dipole and quadrupole moments of water vapor, and the quadrupole moment of nitrogen are listed in Table 1.

The atom–atom potential is defined as the sum of pairwise Lennard–Jones 6–12 interactions [80] between atoms of the radiating molecule and the perturbing molecule, N_2. The Lennard–Jones parameters for the atomic pairs, the ε_{ij} and σ_{ij}, are usually constructed from homonuclear-atom–atom parameters, ε_i and σ_i, by "combination rules" [81–84]. The use of different combination rules and sources of data can yield values of ε_{ij} and σ_{ij} that differ significantly. Hence, these parameters are generally adjusted if reliable experimental data are available. Here, these parameters are adjusted to fit some 177 measured half-widths and 163 line shifts as described below.

Table 1
Values of electrostatic moments for H_2O, N_2.

Molecule	Multipole moment (esu)	Refs.
H_2O	$\mu = 1.8549 \times 10^{-18}$	[76]
	$Q_{xx} = -0.13 \times 10^{-26}$	[77]
	$Q_{yy} = -2.5 \times 10^{-26}$	[77]
	$Q_{zz} = 2.63 \times 10^{-26}$	[77]
N_2	$Q_{zz} = -1.4 \times 10^{-26}$	[78]

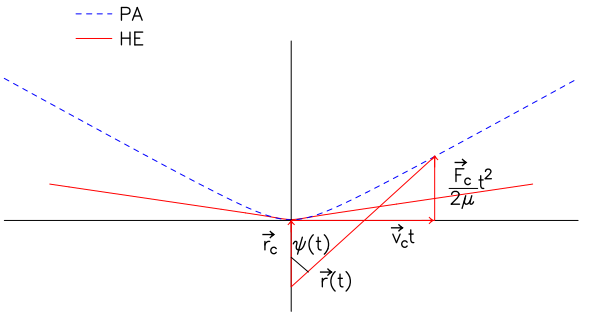

Fig. 1. Robert–Bonamy PA trajectory model (dashed line) compared with the real trajectory (solid line).

The atom–atom distance, r_{ij}, is expressed in terms of the center of mass separation, R, via the expansion in $1/R$ of Sack [85]. The expansion is truncated at an *order* and *rank* (see Ref. [72] for details). Here the formulation of Neshyba and Gamache [26] expanded to twentieth *order* and *rank* 4 is used.

The isotropic part of the expanded atom–atom short range potential is then used to define the curved trajectories used in our calculations.

2.2. Trajectory models

Most of the previous calculations within the CRB formalism employed the RB parabolic trajectory model [16]. In this model the isotropic part of the intermolecular potential is taken into account in determining the distance $\vec{r_c}$, the velocity $\vec{v_c}$, and the force, $\vec{F(r_c)}$, at closest approach. Expanding to second order in time, the trajectory is defined by

$$\vec{r(t)} \cong \vec{r_c} + \vec{v_c} t + \frac{\vec{F(r_c)}}{\mu} \frac{t^2}{2} \quad (2)$$

where μ is the reduced mass of the system. Within the Robert–Bonamy formalism, the trajectories are in a plane and can be described by the intermolecular distance $R(t)$ and the collision angle $\psi(t)$ (Fig. 1). Within the parabolic model, $R(t)$ and $\psi(t)$ can be expressed as

$$R(t) = \sqrt{r_c^2 + v_c'^2 t^2}; \quad \psi(t) = v_c t / \sqrt{r_c^2 + v_c'^2 t^2} \quad (3)$$

with the constraint $\sin^2\psi(t) + \cos^2\psi(t) = 1$. This constraint must be enforced since the sine can become larger than one for large values of r_c because the approximation is

only valid to second order in time. In the model, the true trajectory is replaced by an approximate parabolic trajectory with an effective relative velocity $\vec{v_c'}$ given by

$$v_c' = v_c\left\{1+\frac{8\varepsilon}{\mu v^2}\left[5\left(\frac{\sigma}{r_c}\right)^{12}-2\left(\frac{\sigma}{r_c}\right)^{6}\right]\right\}^{1/2} \quad (4)$$

where ε and σ are the molecular parameters of the isotropic 6–12 Lennard–Jones potential. Within this analytical model, the classical parameters b, v can be replaced by r_c, v_c using the conservation of momentum and the conversation of energy [16].

This model corresponds to approximated solutions at the second order of the classical dynamical equations of motion, from here on designated PA. More realistic trajectories can be obtained by solving Hamilton's equations of motion (HE model). For a given time t, considering the Hamiltonian H formed by the kinetic energy and the isotropic Lennard–Jones potential, the Cartesian components of the trajectories X_i are obtain by solving the system of equations

$$\frac{d}{dt}X_i = \frac{\partial H}{\partial P_i};\quad \frac{d}{dt}P_i = -\frac{\partial H}{\partial X_i};\quad i=1,\ldots,4 \quad (5)$$

where P_i is the conjugate momentum of X_i. The odd and even values of the index i refer to the parallel and perpendicular component of the trajectories in the plane, respectively. The initial conditions X_i^0, P_i^0 have to be given in order to describe the correct relative motion of the perturber and the radiator, which can be seen as the motion of an effective particle with a reduced mass around the center of mass. From the solutions of Hamilton's equations, the trajectories are calculated by

$$R(t) = \sqrt{(X_1-X_3)^2+(X_2-X_4)^2}$$
$$\psi(t) = \mathrm{Arctan}((X_2-X_4)/(X_1-X_3)) \quad (6)$$

The closest approach geometry was chosen as the origin of the frame by defining the conditions $R(0)=r_c;\quad \psi(0)=0$. The closest approach distance and angle are determined numerically by this procedure using a fine time grid. In order to determine accurately those parameters, the grid step is reduced around the closest approach geometry. The differential equations algorithm of Shampine and Gordon [86] is used to perform the numerical integration of Hamilton's equations described in Eq. (5). From the distance of closest approach, the trajectory for the positive times is determined by the same procedure but at predetermined time steps up to the maximum time value chosen for the numerical integration (input to the codes). The trajectory is then symmetrized around the closest approach geometry to yield the complete numerical trajectory. Note that in this case, the distance at closest approach r_c is no longer a meaningful parameter, and the integration in Eq. (1) must be done over the b, v parameters.

3. Calculations

Initial HE calculations were done using the CRB formalism for N_2-broadening of water. Following the study of Ma et al. [22], the intermolecular potential was expanded to high *order* and *rank*, 20 4 4, in order to assure the convergence of the half-widths and line shifts. This yields 1073 terms in the potential. The atom–atom parameters of the previous work [87] for the (000)–(000) band of $H_2^{16}O$ were used as starting values and were then adjusted to produce line shape parameters which agree with the experimental data for the half-widths and line shifts taken from the measurement database for H_2O–N_2 [50]. Also included in the fit are the isotropic Lennard–Jones parameters used for the calculation of the trajectories. Their initial values are determined by the fit of the isotropic part of the potential to an effective 6–12 Lennard Jones potential. 177 (163) transitions were included in the fit for the half-widths (line shifts), ranging from 0.016 cm^{-1} atm^{-1} to 0.117 cm^{-1} atm^{-1} (from −0.018 cm^{-1} atm^{-1} to 0.025 cm^{-1} atm^{-1}). The half-widths are taken from Devi et al. [88], Mrowinski [89], Goyette et al. [90], Frenkel and Woods [91], Bauer et al. [92,93], Liebe and Dillon [94], Kasuga et al. [95], Emery [96], Toth [97], Chance et al. [98], Tretyakov et al. [99], Cazzoli et al. [100–102], Seta et al. [103], Koshelev et al. [104], Golubiatnikov [105], Golubiatnikov et al. [106], and Gamache and Laraia [87]. The line shifts are from Toth [97], Tretyakov et al. [99], Koshelev et al. [104], Golubiatnikov [105], Golubiatnikov et al. [106]. Table 2 reports the final values of the fitted parameters. For the half-widths, 99 of the 177 transitions are within 2σ of the experimental errors, and this value is 44 of 169 for the line shifts.

Table 2
H_2O–N_2 atom–atom parameters used in the CRB calculations.

	ε/k_B (K)	σ (Å)
HN	19.539	2.783
ON	41.033	2.583
Trajectory	68.669	3.5827

Using these parameters the half-widths and the line shifts for the 1639 transitions of the (000)–(000) band of $H_2^{16}O$ considered in the previous work [87] are calculated with N_2 as the perturbing gas using the potential expanded at 20th *order* and *rank* 4 and 4; first with the HE trajectory model and next using the RB parabolic approximation. In the present calculations, the average over the Maxwell–Boltzmann distribution of velocities is done and results are presented for seven temperatures: 200, 225, 275, 296, 350, 500, and 700 K.

4. Discussion

In Fig. 2 the percent difference between the half-widths obtained from the parabolic and the HE trajectory models are plotted versus the half-width in cm^{-1} atm^{-1} for the nitrogen-broadening of water. The plot symbols are J''. The general trend from the broad to intermediate to narrow lines is that the percent difference and the spread of the data increase. For the broad lines, the difference is roughly −1%, whereas it reaches almost +5% for the intermediate and −5% for the narrow lines. This indicates that for the transitions with large half-widths the parabolic and HE models give similar results, confirming the

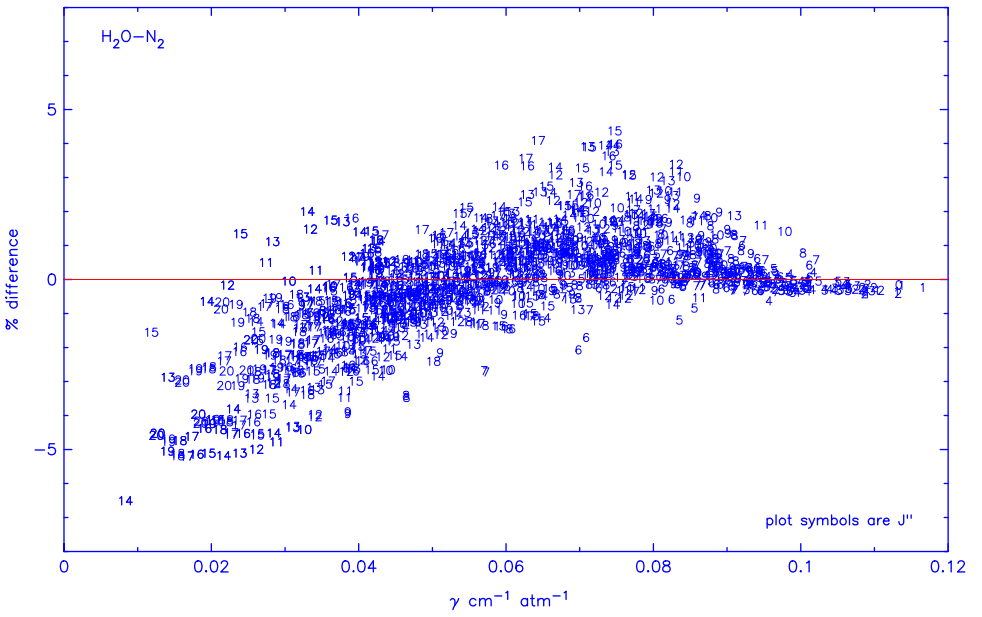

Fig. 2. Percent difference between Hamilton's equations and the parabolic trajectory model calculations of the half-widths versus the half-width for nitrogen broadening of water. The plot symbols are J''.

Table 3
Statistics of the comparison of line half-widths and line shifts for H_2O in collision with N_2 determined from the two trajectory models of this study. For the line shift the deviation, $\delta_{HE}-\delta_{PA}$, is reported in $cm^{-1}\,atm^{-1}$.

Parameter	APD	AAPD	SD	PD_{max}	PD_{min}
γ	−0.30	1.08	1.52	4.24	−6.63
	AD[a]	AAD[a]	$S\tilde{D}$[a]	$(\delta_{HE}-\delta_{PA})_{max}$	$(\delta_{HE}-\delta_{PA})_{min}$
δ	0.712	0.589	0.596	0.00272	−0.00253

[a] $AD=\frac{\sum_{i=1}^{N}(\delta_{meas}-\delta_{calc})}{N}\times 10^2$, $AAD=\frac{\sum_{i=1}^{N}(|\delta_{meas}-\delta_{calc}|)}{N}\times 10^2$, and $S\tilde{D}$ is the standard deviation of AD.

results of Refs. [39,40], however for the intermediate and narrow lines a more realistic trajectory model should be employed. The statistics (percent difference (PD), average absolute percent difference (AAPD), and standard deviation (SD)) of the comparison for the 1639 transitions involved the calculations are presented in Table 3. Plots were also made with the x-axis being $J''+0.1(J''-Ka'')$ with Ka'' as the plot symbols or $Ka''+0.1(J''-Ka'')$ with J'' as the plot symbols to see if structure with respect to the rotational quantum numbers could be detected. Some of these plots are available on one of the authors web site (faculty.uml.edu/Robert_Gamache) Unfortunately, no structure could be detected that would allow the development of propensity rules.

In order to better understand the influence of the trajectory model on these results, the $16_{5\ 11}\leftarrow 16_{4\ 12}$ (hereafter called line 1) and $15_{0\ 15}\leftarrow 14_{1\ 14}$ (hereafter called line 2) transitions of the rotational band of water were studied in detail. These transitions are similar in J'' values but yield about −1.5% and −5.3% difference, respectively, on the half-widths between the two trajectory models. For these two transitions, the imaginary and real parts of $(1-e^{-S})$ as a function of the impact parameter b is plotted in Fig. 3. In the CRB formalism both the real and imaginary parts contribute to the half-width and line shift. However, in this work using the CRB theory for H_2O–N_2 the effect of the imaginary term on the half-width is small [72] hence the focus is on graph on the right-hand-side of Fig. 3. The integrand has very different behavior for the two transitions: for line 1 the integrand reaches 1 (saturates) to about 3 Å whereas for line 2 it never saturates. Notice also that as the real part saturates for line 1 the imaginary part goes to zero.

A comparison of the trajectories obtained from both models for different values of the impact parameter b is presented in Fig. 4. It is observed that as the value of b increases, the difference between the two trajectory models decreases. For larger value of b, the trajectories are exactly the same and as b increases further both models reduce to the straight-line trajectory model. Consequently for line 1, which saturates about 3 Å, the trajectories are similar and the difference between the half-widths from the two models is small. For line 2 the integrand does not saturate and the integral continues to small values of b where the results are sensitive to the details of the short-range atom–atom potential. Here at small impact parameter the differences between the two trajectory models are large, leading to different values of the half-width from the two models.

The differences between the trajectory models are greatest for nearly head-on collisions with small impact parameter b. Meanwhile, as shown in Eq. (1), the integrand of the shift is proportional to $\exp(-ReS_2(b))$ whose magnitudes are close to zero in small b region because $ReS_2(b)$ is larger there. Thus, one expects the effects on the shifts from choosing different trajectory models are less significant than on the half-widths. In addition, one

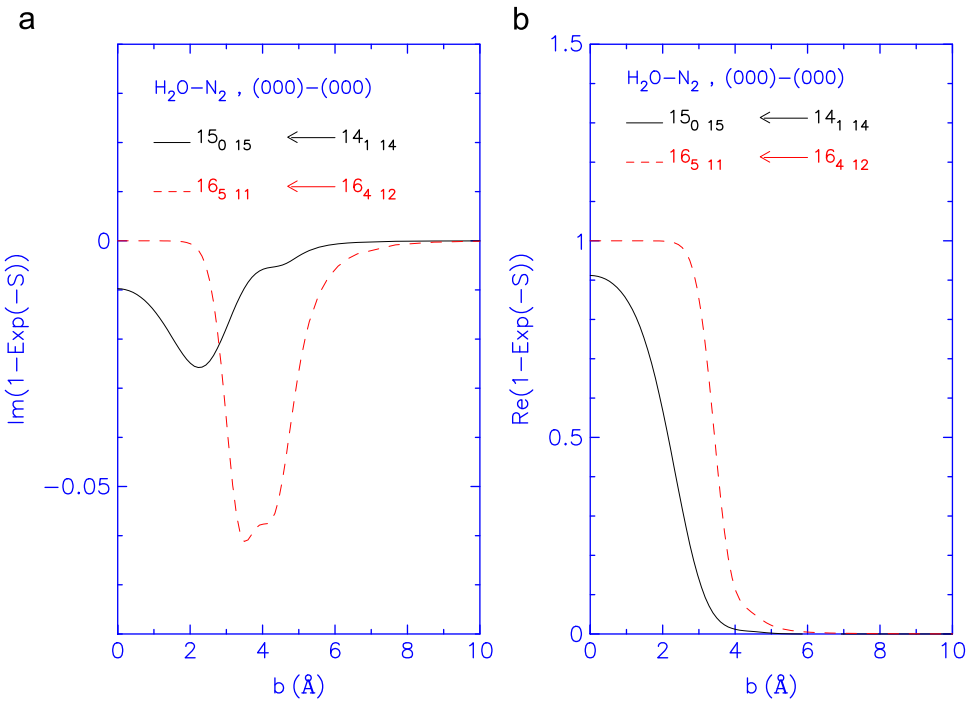

Fig. 3. Imaginary and real parts of $(1-e^{-S})$ for the $16_{5\ 11}\leftarrow16_{4\ 12}$ and $15_{0\ 15}\leftarrow14_{1\ 14}$ N_2-broadened H_2O transitions in the (000)←(000) band versus the impact parameter b (in Angstrom).

expects that in general, calculated shifts are mainly determined by the long-range interactions. However, if percent differences are calculated the range is from −2650% to 600%. In forming the percent difference one divides by the rotational band line shifts (small numbers) which greatly exaggerates the values. A better method is to look at the difference in the line shifts, $\delta_{HE}-\delta_{PA}$ in $cm^{-1}\ atm^{-1}$. Fig. 5 shows the difference, $\delta_{HE}-\delta_{PA}$, in the N_2-induced line shifts calculated using the two trajectory models versus $J''+0.1(J''-Ka'')$, where the second term is to spread out points that have the same J''. The plot symbols in Fig. 5 are Ka_{min} of the transition (minimum of Ka″ and Ka′) to look for structure with respect to the Ka_{min} of the transition. Other plots were made to look at structure with respect to J'' and Ka″. From these plots no apparent structures were found. The range of the deviations in Fig. 5 is small (up to 0.0027 $cm^{-1}\ atm^{-1}$) compared with the average absolute shift (0.007 $cm^{-1}\ atm^{-1}$ for the HE calculations).

The calculations using both trajectory models were compared to the N_2-broadening measurement database [50]. The average percent difference between the calculations and the measurements for each trajectory model are very similar; −5.4 for the HE model and −5.57 for the PA. There is considerable scatter in the measurements [50], which contributes to the similar differences between the two trajectory models. Closer inspection shows that when the difference between the HE and PA calculations is greater than 1.75% the HE calculations are always closer to the measured data. For N_2-broadening of H_2O only the measurements of Toth [97] considered a large number of transitions. These data are also thought to be among the best for the rotational band. Considering Toth's N_2-broadened half-width data (158 transitions) the HE calculations show a −1.86 PD, a 11.07 AAPD, and 17.18 SD compared with −2.01 PD, 12.02 AAPD, and 18.19 SD for the PA calculations. The statistics for comparing with all N_2-broadening measurements are presented in Table 4.

There are less measured data for the line shifts. Table 5 gives the statistics for the comparison of the calculations with these measurements. The HE calculations agree better with the measurements than do the PA calculations.

5. Conclusions

The half-widths and line shifts of 1639 rotational band transitions of water vapor in collision with N_2 were calculated using trajectories determined by solving Hamilton's equations of motion and by the Robert–Bonamy parabolic approximation. The parameters determined from the two trajectory models are compared with each other and with the measurement database. The differences in half-widths between the two trajectory models range from about 5% to −5%. These differences are greater than the current requirements of the spectroscopic and remote sensing communities [56–58]. It is important to note that future missions are already demanding a reduction in these uncertainties. Comparison of the HE and PA calculations with the measurement databases reveals that the HE calculations show better agreement with measurements for both the half-width and the line shift.

Despite the fact that the HE trajectory solutions are computationally more intense, theoretical calculations of

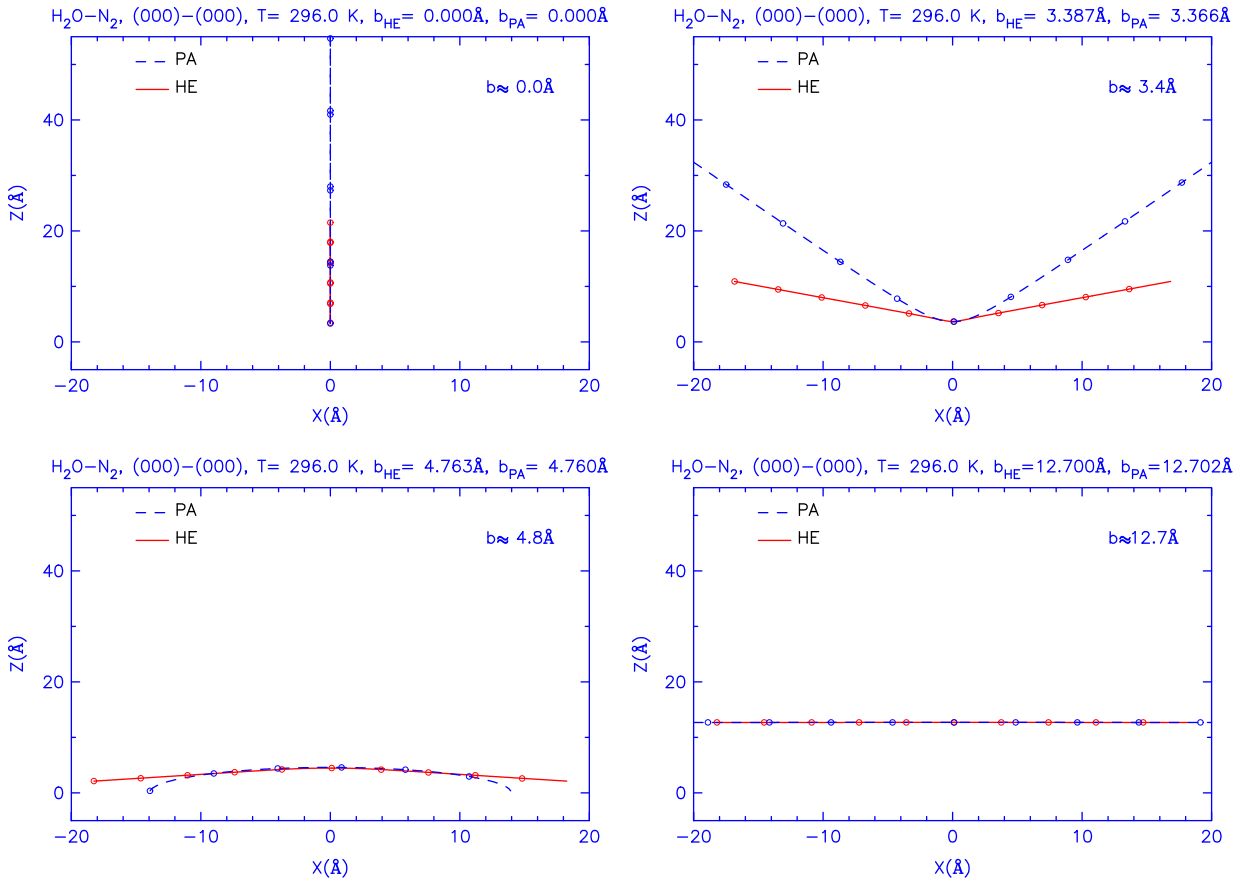

Fig. 4. Comparison of the trajectories obtained from Hamilton's equations and parabolic trajectory model for different values of the impact parameter b (in Angstrom).

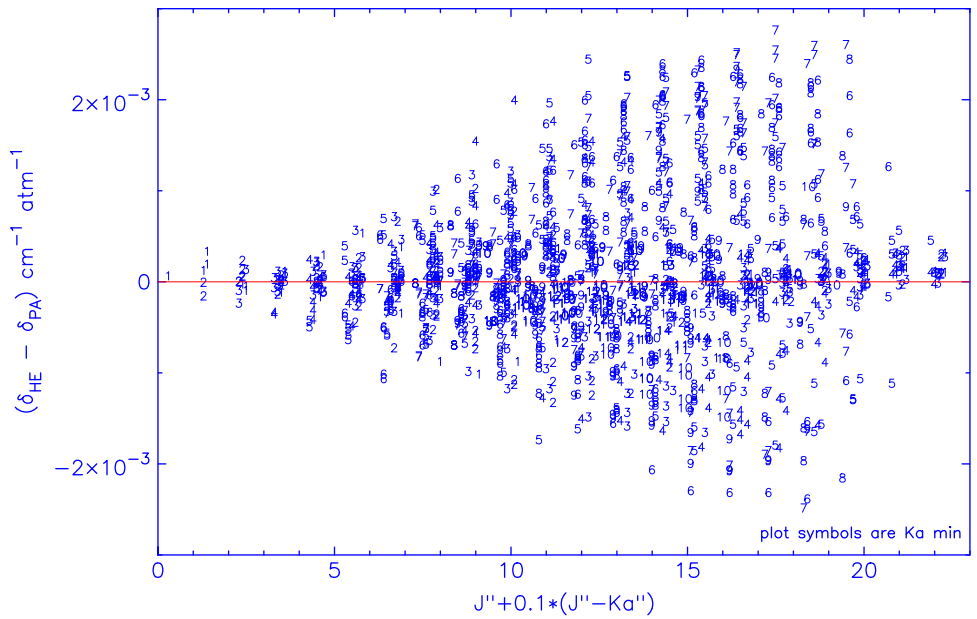

Fig. 5. Deviation, $\delta_{HE}-\delta_{PA}$, between Hamilton's equations and the parabolic trajectory model calculations of the line shifts versus $J''+0.1(J''-\mathrm{Ka}'')$ for nitrogen broadening of water. The plot symbols are Ka_{min}.

Table 4
Statistics of the comparison of measured half-width data with the half-width parameters determined from the two trajectory models of this study for N_2-broadening of H_2O.

Refs.	# Points	HE			PA		
		PD	AAPD	SD	PD	AAPD	SD
[107]	17	0.99	8.94	12.66	0.68	8.79	12.85
[108]	7	−39.12	51.58	62.62	−41.04	54.25	65.16
[109]	15	29.82	29.82	16.08	30.02	30.02	15.99
[110]	3	28.05	28.05	10.64	27.70	27.70	10.72
[97]	158	−1.86	11.07	17.18	−2.01	12.02	18.19
[111]	42	−34.70	34.85	37.42	−34.68	34.88	38.22
[103]	2	−0.31	1.17	–	−0.76	1.09	–
[104]	3	3.64	3.64	–	3.60	3.60	–
[101]	5	8.34	8.34	4.59	8.11	8.11	4.66

Table 5
Statistics of the comparison of measured line shift data with the line shape parameters determined from the two trajectory models of this study for H_2O in collision with N_2.

Refs.	# Data	HE			PA		
		AD[a]	AAD[a]	$S\tilde{D}$[a]	AD[a]	AAD[a]	$S\tilde{D}$[a]
[97]	158	−0.105	0.345	0.435	−0.197	0.712	0.891
[104]	3	−0.0263	0.140	–	−0.0767	0.305	–
[106]	2	−0.0180	0.0250	–	−0.0070	0.0500	–

[a] See Table 3 for definitions.

the line shape parameters must employ this model if the needs of the remote sensing community are to be met. As a result of this study, our line shape codes now use Hamilton's equations for the trajectory model.

Acknowledgment

JL, RRG, ALL are pleased to acknowledge support of this research by the National Science Foundation through Grant no. ATM-0803135. QM and RT acknowledge financial support from NASA under Grants NNG06GB23G, NNX09AB62G, and FCCS-547. Any opinions, findings, and conclusions or recommendations expressed in this material are those of the author(s) and do not necessarily reflect the views of the National Science Foundation or NASA.

References

[1] Anderson PW. Pressure broadening in the microwave and infrared regions. Physical Review 1949;76:647–61.
[2] Anderson PW. Physics. Dissertation. Harvard University; 1949.
[3] Tsao CJ, Curnutte B. Line-widths of pressure-broadened spectral lines. Journal of Quantitative Spectroscopy and Radiative Transfer 1962;2:41–91.
[4] Leavitt RP. Pressure broadening and shifting in microwave and infrared spectra of molecules of arbitrary symmetry: an irreducible tensor approach. Journal of Chemical Physics 1980;73:5432–50.
[5] Hartmann J-M, Boulet C, Robert D. In: Collisional effects on molecular spectra: laboratory experiments and models, consequences for applications. Amsterdam: Elsevier Science; 2008.
[6] Buldyreva J, Lavrentieva N, Starikov V. In: Collisional line broadening and shifting of atmospheric gases. A practical guide for line shape modelling by current semi-classical approaches. Singapore: World Scientific Publishing Co.; 2010.
[7] Davies RW. Many-body treatment of pressure shifts associated with collisional broadening. Physical Review A 1975;12:927–46.
[8] Davies RW, Oli BA. Theoretical calculations of H_2O linewidths and pressure shifts: comparison of the Anderson theory with quantum many-body theory for N_2 and air-broadened lines. Journal of Quantitative Spectroscopy and Radiative Transfer 1978;20:95–120.
[9] Oka T. In: Bates DR, editor. Advances in atomic and molecular physics. New York: Academic Press; 1973.
[10] Tipping RH. Impact theory for the noble gas pressure-induced line widths and shifts of HCl spectral lines. Ph.D. dissertation. Department of Physics, The Pennsylvania State University; 1969.
[11] Tipping RH, Herman RM. Impact theory for the noble gas pressure-induced HCl vibration–rotation and pure rotation line widths—I. Journal of Quantitative Spectroscopy and Radiative Transfer 1970;10:881–96.
[12] Herman RM, Tipping RH. Impact theory for the noble gas pressure-induced HCl vibration–rotation and pure rotation line shifts—II. Journal of Quantitative Spectroscopy and Radiative Transfer 1970;10:897–908.
[13] Neilsen WB, Gordon RG. On a semiclassical study of molecular collisions. I. General method. Journal of Chemical Physics. 1973;58:4131–6.
[14] Smith EW, Giraud M, Cooper JA. Semiclassical theory for spectral line broadening in molecules. Journal of Chemical Physics 1976;65:1256–67.
[15] Bonamy J, Bonamy L, Robert D. Overlapping effects and motional narrowing in molecular band Shapes: application to the Q branch of HD. Journal of Chemical Physics 1977;67:4441–53.
[16] Robert D, Bonamy J. Short range force effects in semiclassical molecular line broadening calculations. Journal de Physique (France) 1979;40:923–43.
[17] Leavitt RP, Korff D. Cut-off-free theory of impact broadening and shifting in microwave and infrared gas spectra. Journal of Chemical Physics 1981;74:2180–98.
[18] Looney JP, Herman RM. Air broadening of the hydrogen halide—I. N_2-broadening and shifting in the HCl fundamental. Journal of Quantitative Spectroscopy and Radiative Transfer 1987;37:547–57.
[19] Berard M, Lallemand P. Influence of the use of approximate trajectories for binary collision calculations. Journal of Quantitative Spectroscopy and Radiative Transfer 1978;19:387–96.
[20] Gamache RR, Davies RW. Theoretical N_2-, O_2-, and air-broadened halfwidths of $^{16}O_3$ calculated by quantum Fourier transform theory with realistic collision dynamics. Journal of Molecular Spectroscopy 1985;109:283–99.
[21] Tejwani GDT. Improved calculated linewidths for H_2O broadened by N_2. Journal of Quantitative Spectroscopy and Radiative Transfer 1988;40:605–12.
[22] Ma Q, Tipping RH, Gamache RR. Uncertainties associated with theoretically calculated N_2-broadened half-widths of H_2O lines. Molecular Physics 2010;108:2225–52.
[23] Kubo R. Generalized cumulant expansion method. Journal of Physical Society of Japan 1962;17:1100–20.
[24] Labani B, Bonamy J, Robert D, Hartmann J-M, Taine J. Collisional broadening of rotation–vibration lines for asymmetric top molecules I. Theoretical model for both distant and close collisions. Journal of Chemical Physics 1986;84:4256–67.
[25] Labani B, Bonamy J, Robert D, Hartmann J-M. Collisional broadening of rotation–vibration lines for asymmetric-top molecules III. Self-broadening case; application to H_2O. Journal of Chemical Physics 1987;87:2781–9.
[26] Neshyba SP, Gamache RR. Improved line broadening coefficients for asymmetric rotor molecules: application to ozone perturbed by nitrogen. Journal of Quantitative Spectroscopy and Radiative Transfer 1993;50:443–53.
[27] Neshyba SP, Lynch R, Gamache RR, Gabard T, Champion J-P. Pressure induced widths and shifts for the ν_3 band of methane. Journal of Chemical Physics 1994;101:9412–21.
[28] Gabard T. Argon-broadened line parameters in the band of $^{12}CH_4$. Journal of Quantitative Spectroscopy and Radiative Transfer 1997;57:177–96.
[29] Gamache RR, Lacome N, Pierre G, Gabard T. Nitrogen broadening of SF_6 transitions in the ν_3 band. Journal of Molecular Structure 2001;599:279–92.
[30] Boudon V, Champion J-P, Gabard T, Löete M, Michelot F, Pierre G, Rotger M, Wenger C, Rey M. Symmetry-adapted tensorial formalism

to model rovibrational and rovibronic spectra of molecules pertaining to various point groups. Journal of Molecular Spectroscopy 2004;228:620–34.
[31] Lynch R, Gamache RR, Neshyba SP. Fully complex implementation of the Robert–Bonamy formalism: halfwidths and line shifts of H_2O broadened by N_2. Journal of Chemical Physics 1996;105: 5711–21.
[32] Goldstein H. In: Classical mechanics. Cambridge, MA: Addison-Wesley; 1950.
[33] Bykov AD, Lavrentieva NN, Sinitsa LN. Resonance functions of the theory of broadening and shift of lines for actual trajectories. Atmospheric and Oceanic Optics 1992;5:728–30.
[34] Joubert P, Bonamy J, Robert D. Exact trajectory in semiclassical line broadening and line shifting calculation test for H_2–He Q(1) line. Journal of Quantitative Spectroscopy and Radiative Transfer 1999;61:19–24.
[35] Buldyreva J, Bonamy J, Robert D. Semiclassical calculations with exact trajectory for N_2 rovibrational Raman linewidths at temperatures below 300 K. Journal of Quantitative Spectroscopy and Radiative Transfer 1999;62:321–43.
[36] Buldyreva J, Benec'h S, Chrysos M. Oxygen-broadened and air-broadened linewidths for the NO infrared absorption bands by means of the exact-trajectory approach. Physical Review A 2001;63:032705.
[37] Buldyreva J, Nguyen L. On the role of trajectory modeling in the C_2H_2 infrared line-broadening computation. Molecular Physics 2004;102:1523–35.
[38] Afzelius M, Buldyreva J, Bonamy J. Exact treatement of classical trajectories governed by an isotropic for linewidth computations. Molecular Physics 2004;102:1759–65.
[39] Neshyba S, Gamache RR. Comparison of half-widths calculated using trajectories from the parabolic approximation and by solving Hamilton's equations. Unpublished work. University of Massachusetts Lowell; 1995.
[40] Antony BK, Neshyba S, Gamache RR. Self-broadening of water vapor transitions via the complex Robert–Bonamy theory. Journal of Quantitative Spectroscopy and Radiative Transfer 2006;105: 148–63.
[41] Gamache RR, Lamouroux J, Laraia A, Hartmann J-M, Boulet C. Semiclassical calculations of half-widths and line shifts for transitions in the 30012←00001 and 30013←00001 bands of CO_2 I: collisions with N_2. Journal of Quantitative Spectroscopy and Radiative Transfer, this issue.
[42] Lamouroux J, Gamache RR, Laraia AL, Hartmann J-M, Boulet C. Semiclassical calculations of half-widths and line shifts for transitions in the 30012←00001 and 30013←00001 bands of CO_2 II: collisions with O_2 and air, Journal of Quantitative Spectroscopy and Radiative Transfer, this issue.
[43] Bernath PF. The spectroscopy of water vapour: experiment, theory and applications. Physical Chemistry Chemical Physics 2002;4: 1501–9.
[44] Hartmann DL. In: Global physical climatology. Boston: Academic Press, Inc.; 1994.
[45] Rothman LS, Gordon IE, Barbe A, Benner DC, Bernath PF, Birk M, Boudon V, Brown LR, Campargue A, Champion J-P, Chance K, Coudert LH, Dana V, Devi VM, Fally S, Flaud J-M, Gamache RR, Goldman A, Jacquemart D, Kleiner I, Lacome N, Lafferty WJ, Mandin J-Y, Massie ST, Mikhailenko SN, Miller CE, Moazzen-Ahmadi N, Naumenko OV, Nikitin AV, Orphal J, Perevalov VI, Perrin A, Predoi-Cross A, Rinsland CP, Rotger M, Simeckova M, Smith MAH, Sung K, Tashkun SA, Tennyson J, Toth RA, Vandaele AC, Auwera JV. The HITRAN 2008 molecular spectroscopic database. Journal of Quantitative Spectroscopy and Radiative Transfer 2009;110:533–72.
[46] Jacquinet-Husson N, Scott NA, Chedin A, Crepeau L, Armante R, Capelle V, Orphal J, Coustenis A, Boonne C, Poulet-Crovisier N, Barbe A, Birk M, Brown LR, Camy-Peyret C, Claveau C, Chance K, Christidis N, Clerbaux C, Coheur PF, Dana V, Daumont L, De Backer-Barilly MR, Di Lonardo G, Flaud J-M, Goldman A, Hamdouni A, Hess M, Hurley MD, Jacquemart D, Kleiner I, Köpke P, Mandin JY, Massie S, Mikhailenko S, Nemtchinov V, Nikitin A, Newnham D, Perrin A, Perevalov VI, Pinnock S, Régalia-Jarlot L, Rinsland CP, Rublev A, Schreier F, Schult L, Smith KM, Tashkun SA, Teffo J-L, Toth RA, Tyuterev VG, Vander Auwera J, Varanasi P, Wagner G. The GEISA spectroscopic database: current and future archive for Earth and planetary atmosphere studies. Journal of Quantitative Spectroscopy and Radiative Transfer 2008;109:1043–59.
[47] Pumphrey HC, Buehler S. Instrumental and spectral parameters: their effect on and measurement by microwave limb sounding of the atmosphere. Journal of Quantitative Spectroscopy and Radiative Transfer 2000;64:421–37.
[48] Liljegren JC, Boukabara S-A, Cady-Pereira K, Clough SA. The effect of the half-width of the 22-GHz water vapor line on retrievals of temperature and water vapor profiles with a 12-channel microwave radiometer. IEEE Transactions on Geoscience and Remote Sensing 2005;43:1102–8.
[49] Payne VH, Delamere JS, Cady-Pereira KE, Gamache RR, Moncet J-L, Mlawer E, Clough SA. Air-broadened half-widths of the 22 GHz and183 GHz water vapor lines. IEEE Transactions in Geoscience and Remote Sensing 2007;46:3601–17.
[50] Gamache RR, Hartmann J-M. An intercomparison of measured pressure-broadening and pressure-shifting parameters of water vapor. Canadian Journal of Chemistry 2004;82:1013–27.
[51] Benedict WS, Kaplan LD. Calculation of line widths in H_2O–H_2O and H_2O–O_2 collisions. Journal of Quantitative Spectroscopy and Radiative Transfer 1964;4:453–69.
[52] Benedict WS, Kaplan LD. Calculation of line widths in H_2O–H_2O and H_2O–O_2 collisions. Journal of Quantitative Spectroscopy and Radiative Transfer 1964;4:453–69.
[53] Gamache RR, Fischer J. Half-widths of $H_2^{16}O$, $H_2^{18}O$, $H_2^{17}O$, $HD^{16}O$, and $D_2^{16}O$: I. Comparison between isotopomers. Journal of Quantitative Spectroscopy and Radiative Transfer 2003;78:289–304.
[54] Gamache RR, Davies RW. Theoretical calculations of N_2-broadened halfwidths of H_2O using quantum Fourier transform theory. Applied Optics 1983;22:4013–9.
[55] Gamache RR, Fischer J. Half-widths of $H_2^{16}O$, $H_2^{18}O$, $H_2^{17}O$, $HD^{16}O$, and $D_2^{16}O$: II. Comparison with measurements. Journal of Quantitative Spectroscopy and Radiative Transfer 2003;78:305–18.
[56] Barbe A, editor. Proceedings of the atmospheric spectroscopy applications workshop. ASA REIMS 96. Champagne Ardenne: Université de Reims; 1996.
[57] Smith M.A.H. editor. NASA conference publication 2396. NASA; 1985.
[58] Smith M.A.H.. Third Langley spectroscopic parameters workshop. Hampton, VA: NASA Langley Research Center; 1992.
[59] Gamache RR, Rosenmann L. The effects of velocity averaging in broadening coefficient calculations. Journal of Molecular Spectroscopy 1994;164:489–99.
[60] Wagner G, Birk M, Gamache RR, Hartmann J-M. Collisional parameters of H_2O lines: effects of temperature. Journal of Quantitative Spectroscopy and Radiative Transfer 2005;92:211–30.
[61] Mandin J-Y, Chevillard J-P, Flaud J-M, Camy-Peyret C. N_2 broadening coefficients of $H_2^{16}O$ lines between 8500 and 9300 cm^{-1}. Journal of Molecular Spectroscopy 1988;132:352–60.
[62] Mandin J-Y, Chevillard J-P, Camy-Peyret C, Flaud J-M. N_2-broadening coefficients of $H_2^{16}O$ lines between 9 500 and 11 500 cm^{-1}. Journal of Molecular Spectroscopy 1989;138:272–81.
[63] Grossmann BE, Browell EV. Water-vapor line broadening and shifting by air, nitrogen, oxygen, and argon in the 720-nm wavelength region. Journal of Molecular Spectroscopy 1989;138: 562–95.
[64] Brown LR, Plymate C. H_2-broadened $H_2^{16}O$ in four infrared bands between 55 and 4045 cm^{-1}. Journal of Quantitative Spectroscopy and Radiative Transfer 1996;56:263–82.
[65] Zou Q, Varanasi P. Laboratory measurement of the spectroscopic line parameters of water vapor in the 610–2100 and 3000–4050 cm^{-1} regions at lower-tropospheric temperatures. Journal of Quantitative Spectroscopy and Radiative Transfer 2003;82: 45–98.
[66] Gamache RR, Hartmann J-M, Rosenmann L. Collisional broadening of water-vapor lines: I. A survey of experimental results. Journal of Quantitative Spectroscopy and Radiative Transfer 1994;52: 481–99.
[67] Gamache RR, Hartmann J-M. Collisional parameters of H_2O lines: effects of vibration. Journal of Quantitative Spectroscopy and Radiative Transfer 2004;83:119–47.
[68] Tipping RH, Ma Q. Theoretical calculation of the N_2 broadened half-widths OF H_2O. In: Proceedings of 65th international symposium on molecular spectroscopy. The Ohio State University; 2010.
[69] Lamouroux J, Gamache RR, Laraia AL, Ma Q, TIpping RH. The importance of trajectory models in complex Robert–Bonamy formalism calculations: application to the rotational band of H_2O broadened by N_2, O_2, and air. In: Proceedings of 20th international conference on spectral line shapes. St. John's, Newfoundland, Canada; 2010.
[70] Lynch R. Half-widths and line shifts of water vapor perturbed by both nitrogen and oxygen. PhD dissertation. Physics Department, University of Massachusetts Lowell; 1995.

[71] Gamache RR, Lynch R, Neshyba SP. New developments in the theory of pressure-broadening and pressure-shifting of spectral Lines of H_2O: the complex Robert–Bonamy formalism. Journal of Quantitative Spectroscopy and Radiative Transfer 1998;59:319–35.
[72] Lynch R, Gamache RR, Neshyba SP. N_2 and O_2 induced halfwidths and line shifts of water vapor transitions in the (301)←(000) and (221)←(000) bands. Journal of Quantitative Spectroscopy and Radiative Transfer 1998;59:595–613.
[73] Watson JKG. Determination of centrifugal distortion coefficients of asymmetric-top molecules. Journal of Chemical Physics 1967;46:1935–49.
[74] Matsushima F, Odashima H, Iwaskai T, Tsunekawa S. Frequency measurement of pure rotational transitions of H_2O from 0.5 to 5 THz. Journal of Molecular Structure 1995;352–353:371–8.
[75] Huber KP, Herzberg G. In: Molecular spectra and molecular structure: constants of diatomic molecules. New York: Van Nostrand; 1979.
[76] Shostak SL, Muenter JS. The dipole moment of water. II. Analysis of the vibrational dependence of the dipole moment in terms of a dipole moment function. Journal of Chemical Physics 1991;94:5883–90.
[77] Flygare WH, Benson RC. The molecular Zeeman effect in diamagnetic molecules and the determination of molecular magnetic moments (g values), magnetic susceptibilities, and molecular quadrupole moments. Molecular Physics 1971;20:225–50.
[78] Mulder F, van Dijk G, van der Avoird A. Multipole moments, polarizabilities and anisotropic long range interaction coefficients for N_2. Molecular Physics 1980;39:407–25.
[79] Stogryn DE, Stogryn AP. Molecular multipole moments. Molecular Physics 1966;11:371–93.
[80] Jones JE. On the determination of molecular fields. II. From the equation of state of a gas. Proceedings of the Royal Society A 1924;106:463–77.
[81] Hirschfelder JO, Curtiss CF, Bird RB. In: Molecular theory of gases and liquids. New York: Wiley; 1964.
[82] Diaz Pena M, Pando C, Renuncio JAR. Combination rules for intermolecular potential parameters. I. Rules based on approximations for the long-range dispersion energy. Journal of Chemical Physics 1982;76:325–32.
[83] Diaz Pena M, Pando C, Renuncio JAR. Combination rules for intermolecular potential parameters. II. Rules based on approximations for the long-range dispersion energy and an atomic distortion model for the repulsive interactions. Journal of Chemical Physics 1982;76:333–9.
[84] Good RJ, Hope CJ. Test of combining rules for intermolecular distances. Potential function constants from second virial coefficients. Journal of Chemical Physics. 1971;55:111–6.
[85] Sack RA. Two-center expansion for the powers of the distance between two points. Journal of Mathematical Physics 1964;5:260–8.
[86] Shampine L, Gordon M. In: Computer solution of ordinary differential equations: the initial value problem.Freeman; 1975.
[87] Gamache RR, Laraia AL. N_2-, O_2-, and air-broadened half-widths, their temperature dependence, and line shifts for the rotation band of $H_2^{16}O$. Journal of Molecular Spectroscopy 2009;257:116–27.
[88] Devi VM, Benner DC, Rinsland CP, Smith MAH, Sidney BD. Diode laser measurements of air and nitrogen broadening in the ν_2 bands of HDO, $H_2^{16}O$, and $H_2^{18}O$. Journal of Molecular Spectroscopy 1986;117:403–7.
[89] Mrowinski D. Refraction and absorption in atmospheric gases near the 22 GHz water vapour rotational line. Zeitschrift für Angewandte Physik 1970;29:323–30.
[90] Goyette TM, Lucia FCD, Dutta JM, Jones CR. Variable temperature pressure broadening of the 41,4–32,1 transition of H_2O by O_2 and N_2. Journal of Quantitative Spectroscopy and Radiative Transfer 1993;49:485–9.
[91] Frenkel L, Woods D. The microwave absorption by H_2O vapor and its mixtures with other gases between 100 and 300-Gc/s. Proceedings of IEEE 1966;54:498–505.
[92] Bauer A, Godon M, Kheddar M, Hartmann J-M, Bonamy J, Robert D. Temperature and perturber dependences of water-vapor 380 GHz-line broadening. Journal of Quantitative Spectroscopy and Radiative Transfer 1987;37:531–9.
[93] Bauer A, Godon M, Kheddar M, Hartmann J-M. Temperature and perturber dependences of water vapor line-broadening. Experiments at 183 GHz; calculations below 1000 GHz. Journal of Quantitative Spectroscopy and Radiative Transfer 1989;41:49–54.
[94] Liebe HJ, Dillon TA. Accurate foreign-gas-broadening parameters of the 22-GHz H_2O line from refraction spectroscopy. Journal of Chemical Physics 1969;50:727–32.
[95] Kasuga T, Kuze H, Shimizu T. Determinations of relaxation rate constants on the 22 GHz rotational transition of H_2O by coherent transient spectroscopy. Journal of Chemical Physics 1978;69:5195–8.
[96] Emery R. Atmospheric absorption measurements in the region of 1 mm wavelength. Infrared Physics 1972;12:65–79.
[97] Toth RA. Air- and N_2-broadening parameters of water vapor: 604 to 2271 cm^{-1}. Journal of Molecular Spectroscopy 2000;201:218–43.
[98] Chance KV, Park K, Evenson KM. Pressure broadening of far infrared rotational transitions: 88.65 cm^{-1} H_2O and 114.47 cm^{-1} O_3. Journal of Quantitative Spectroscopy and Radiative Transfer 1998;59:687–8.
[99] Tretyakov MY, Parshin VV, Koshelev MA, Shanin VN, Myasnikova SE, Krupnov AF. Studies of 183 GHz water line: broadening and shifting by air, N_2 and O_2 and integral intensity measurements. Journal of Molecular Spectroscopy 2003;218:239–45.
[100] Cazzoli G, Puzzarini C, Buffa G, Tarrini O. Experimental and theoretical investigation on pressure-broadening and pressure-shifting of the 22.2 GHz line of water. Journal of Quantitative Spectroscopy and Radiative Transfer 2007;105:438–49.
[101] Cazzoli G, Puzzarini C, Buffa G, Tarrini O. Pressure-broadening of water lines in the THz frequency region: improvements and confirmations for spectroscopic databases. Part I. Journal of Quantitative Spectroscopy and Radiative Transfer 2008;109:2820–31.
[102] Cazzoli G, Puzzarini C, Buffa G, Tarrini O. Pressure-broadening of water lines in the THz frequency region: the 1.113 THz line of water. Journal of Quantitative Spectroscopy and Radiative Transfer 2008;109:1563–74.
[103] Seta T, Hoshina H, Kasai Y, Hosako I, Otani C, Loβow S, Urban J, Ekström M, Eriksson P, Murtagh D. Pressure broadening coefficients of the water vapor lines at 556.936 and 752.033 GHz. Journal of Quantitative Spectroscopy and Radiative Transfer 2008;109:144–50.
[104] Koshelev MA, Tretyakov MY, Golubiatnikov Y, Parshin VV, Markov VN, Koval IA. Broadening and shifting of the 321-, 325-, and 380-GHz lines of water vapor by pressure of atmospheric gases. Journal of Molecular Spectroscopy 2007;241:101–8.
[105] Golubiatnikov Y. N_2-, O_2-, and air-broadened half-widths, their temperature dependence, and line shifts for the rotation band of $H_2^{16}O$. Journal of Molecular Spectroscopy 2005;230:196–8.
[106] Golubiatnikov Y, Koshelev MA, Krupnov AF. Pressure shift and broadening of 110–101 water vapor lines by atmosphere gases. Journal of Quantitative Spectroscopy and Radiative Transfer 2008;109:1828–33.
[107] Gasster SD, Townes CH, Goorvitch D, Valero FPJ. Foreign gas collision broadening of the FIR spectrum of water vapor. Journal of the Optical Society of America 1988;5:593–601.
[108] Eng RS, Mantz AW. Tunable diode laser measurement of water vapor line parameters in the 10- to 15-μu spectral region. Journal of Molecular Spectroscopy 1979;74:388–99.
[109] Izatt JR, Sakai H, Benedict WS. Positions, intensities, and widths of water-vapor lines between 475 and 692 cm^{-1}. American Journal of Optical Society 1969;59:19–26.
[110] Sanderson RB, Ginsburg N. Line widths and line strengths in the rotational spectrum of water vapor. Journal of Quantitative Spectroscopy and Radiative Transfer 1963;3:435–44.
[111] Steyert DW, Wang WF, Sirota JM, Donahue NM, Reuter DC. Pressure broadening coefficients for rotational transitions of water in the 380–600 cm^{-1} range. Journal of Quantitative Spectroscopy and Radiative Transfer 2002;72:775–82.